

Progressive fracture analysis of concrete using finite elements with embedded displacement discontinuity

Ha-Won Song[†], Byul Shim[‡], Seung-Min Woo[‡] and Ja-Choon Koo[‡]

Department of Civil Engineering, Yonsei University, Seoul 120-749, Korea

Abstract. In this paper, a finite element with embedded displacement discontinuity which eliminates the need for remeshing of elements in the discrete crack approach is applied for the progressive fracture analysis of concrete structures. A finite element formulation is implemented with the extension of the principle of virtual work to a continuum which contains internal displacement discontinuity. By introducing a discontinuous displacement shape function into the finite element formulation, the displacement discontinuity is obtained within an element. By applying either a nonlinear or an idealized linear softening curve representing the fracture process zone (FPZ) of concrete as a constitutive equation to the displacement discontinuity, progressive fracture analysis of concrete structures is performed. In this analysis, localized progressive fracture simultaneous with crack closure in concrete structures under mixed mode loading is simulated by adopting the unloading path in the softening curve. Several examples demonstrate the capability of the analytical technique for the progressive fracture analysis of concrete structures.

Key words: embedded displacement discontinuity; progressive fracture analysis; concrete structures; finite element method; discontinuous displacement shape function; softening curves; fracture process zone.

1. Introduction

The progressive fracture analysis of concrete structures can be performed effectively by modeling concrete's fracture process zone during crack initiation and propagation. Two main approaches to the finite element fracture analysis of concrete structures are the smeared crack approach, which treats a cracked material as an equivalent continuum, and the discrete crack approach, which regards a crack as an inter-element displacement discontinuity. Several versions of smeared crack models have been proposed: the fixed crack model (Rashid 1968, Cervenka 1970), the rotating crack model (Cope *et al.* 1980) and the multiple fixed crack model (de Borst and Nauta 1985, Okamura and Maekawa 1991). Although these smeared crack models have been widely used in the fracture analysis of concrete, they can not simulate the actual formation of discrete cracks. The discrete crack approach (Ngo and Scordelis 1967) can do this, but the complexities in implementation, such as continuous remeshing or addition of new nodes, and the constraint on the direction of crack propagation along element boundaries are major drawbacks (Bocca 1991). As an attempt to remove these drawbacks, a new approach has been proposed recently to model a crack as a displacement discontinuity within an element. For the so-called embedded crack approach, an extended principle of virtual work for a continuum with an internal displacement discontinuity was utilized for

[†] Associate Professor

[‡] Graduate Research Assistant

embedding the discontinuity within an element (Wan *et al.* 1990, Dvorkin and Assanelli 1991) and another extension of the three-field Hu-Washizu variational statement for a continuum with an internal discontinuity was also utilized recently for formulating elements with a discontinuous displacement field (Lofti and Shing 1995).

In this paper, analysis technique using finite elements embedded displacement discontinuity is applied to the analysis of progressive fractures in concrete. The technique in this paper was initially proposed for the analysis of the shear band in geomaterials by Wan *et al.* (1990). The embedded discontinuous finite element is a pseudo discrete crack element without the difficulties associated with using the discrete crack approach. More specifically, a discontinuous shape function for this element circumvents the aforementioned drawbacks in the discrete crack approach. Our research focuses on the application of Wan *et al.*'s embedded crack approach to the analysis of concrete structures. A softening curve which can be obtained from experimental data on the Fracture Process Zone (FPZ) is utilized for constitutive equation of the discontinuous line. Then, the results obtained using linear and nonlinear softening curve are compared. Also, a localization algorithm is utilized by simultaneously using the unloading behavior of a crack closing with the loading behavior of a crack opening in localized failure analysis. A rational method based on the embedded crack approach suitable for the analysis of progressive fracture in concrete structures under general loading and boundary condition is thus established. Several case studies including types of softening curves and the unloading path in the tension softening behavior are examined.

2. Formulation of progressive fracture

2.1 Modified virtual work

The modified form of the principle of virtual work (Malvern 1969) can be obtained by applying the principle of virtual work to each continuum which has been divided into two parts by a discontinuous line, as shown in Fig. 1.

By applying the modified form of the principle of virtual work to a continuum Ω containing a discontinuous line Γ_{sb} , we obtain

$$\int_{\Omega} \delta \varepsilon_{ij} \sigma_{ij} d\Omega = \int_{\Gamma} \delta u_i \bar{T}_i d\Gamma + \int_{\Omega} \delta u_i f_i d\Omega + \int_{\Gamma_{sb}} \delta d_i t_i d\Gamma \quad (1)$$

where σ_{ij} is stress in the continuum, $\delta \varepsilon_{ij}$ is virtual strain, f_i is body force, δu_i represents the virtual displacement, \bar{T}_i is the traction acting on the continuum boundary Γ , and t_i and δd_i are traction and virtual embedded discontinuous displacement acting on the embedded discontinuous line Γ_{sb} , respectively.

The constitutive equations for the continuum and the discontinuous line can be written as Eqs. (2a) and (2b), respectively.

$$\Delta \sigma_{ij} = L_{ijkl} \Delta \varepsilon_{kl} \quad (2a)$$

$$\Delta t_i = -\eta_{ij} \Delta d_j \quad (2b)$$

where L_{ijkl} is the elastic constitutive tensor of continuum and η_{ij} is the second order tensor which represents constitutive relation along the discontinuous line Γ_{sb} . For the progressive fracture analysis of concrete structure, softening curves which characterizes concrete's fracture process zone and

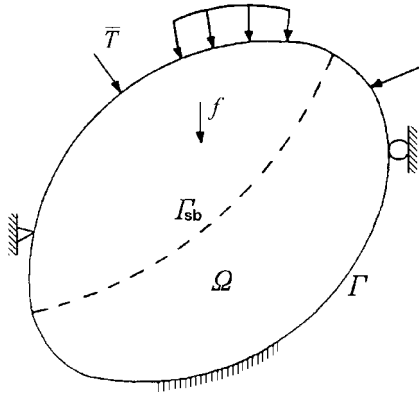


Fig. 1 Continuum with embedded discontinuous line

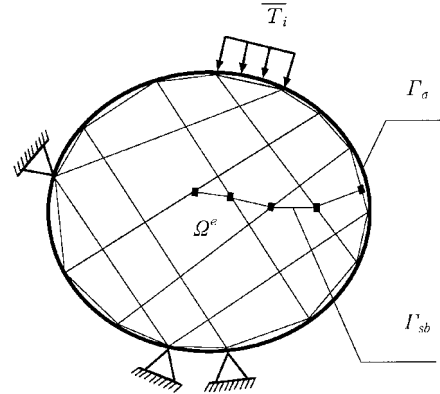


Fig. 2 Finite element discretization of domain

assures a correct energy dissipation during fracture are applied as a constitutive equation for this embedded discontinuous line.

If Eq. (1) is modified into an incremental form by using Eqs. (2), the modified incremental form of the principle of virtual work is obtained as

$$\int_{\Omega'} \delta(\Delta \epsilon_{ij}) L_{ijkl} \Delta \epsilon_{kl} d\Omega = \int_{\Omega'} \delta(\Delta u_i) \Delta f_i d\Omega + \int_{\Gamma_\sigma} \delta(\Delta u_i) \Delta \bar{T}_i d\Gamma + \int_{\Gamma_{sb}} \delta(\Delta d_i) \eta_{ij} \Delta d_j d\Gamma. \quad (3)$$

Eq. (3) can be used for the finite element formulation for progressive fracture analysis.

2.2 Embedded discontinuous finite element

Using the modified incremental form of the principle of virtual work equation on a continuum with an embedded discontinuity, the element stiffness matrix governing the embedded discontinuous finite element is derived. For the discretization of this element, the continuum displacement domain \$\Omega\$ and embedded discontinuous line \$\Gamma_{sb}\$ can be discretized as shown in Fig. 2.

In the displacement domain of element volume \$\Omega^e\$, displacement increment \$\Delta \mathbf{u}\$ and strain increment \$\Delta \boldsymbol{\epsilon}\$ are expressed with nodal displacement increment \$\Delta \bar{\mathbf{u}}\$ and nodal discontinuous displacement increment \$\Delta \bar{\mathbf{d}}\$. These equations are expressed as

$$\Delta \mathbf{u} = \mathbf{N}^{(\alpha)} \cdot \Delta \bar{\mathbf{u}} + \mathbf{N}^{(\beta)} \cdot \Delta \bar{\mathbf{d}} \quad (4a)$$

$$\Delta \boldsymbol{\epsilon} = \mathbf{B}^{(\alpha)} \cdot \Delta \bar{\mathbf{u}} + \mathbf{B}^{(\beta)} \cdot \Delta \bar{\mathbf{d}} \quad (4b)$$

where superscripts \$\alpha\$ and \$\beta\$ represent continuity and discontinuity, respectively. Here \$\mathbf{N}^{(\alpha)}\$ and \$\mathbf{N}^{(\beta)}\$ are shape functions and \$\mathbf{B}^{(\alpha)}\$ and \$\mathbf{B}^{(\beta)}\$ are compatibility matrices which can be expressed as a differential form of \$\mathbf{N}^{(\alpha)}\$ and \$\mathbf{N}^{(\beta)}\$. Element volume \$\Omega_e\$ is divided into positive element volume \$\Omega_e^+\$ and negative element volume \$\Omega_e^-\$ by embedded discontinuous line \$\Gamma_{sb}\$, as shown in Fig. 3. The embedded shape function \$\mathbf{N}^{(\beta)}\$ of the discontinuous line for a 4-node quadrilateral element and its compatibility matrix \$\mathbf{B}^{(\beta)}\$ can be written as Eqs. (5) and (6), respectively (Wan *et al.* 1990).

$$N_1^{(\beta)+} = \frac{1}{4}(1 - \xi)(1 - \eta) \quad N_1^{(\beta)-} = -\frac{1}{4}(1 + \xi)(1 - \eta)$$

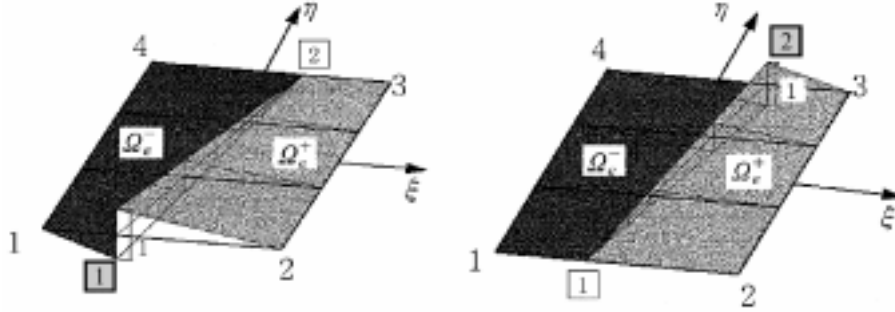


Fig. 3 Discontinuous shape function for a 4-node quadrilateral element

$$N_2^{(\beta)+} = \frac{1}{4}(1 - \xi)(1 + \eta) \quad N_2^{(\beta)-} = -\frac{1}{4}(1 + \xi)(1 + \eta) \tag{5}$$

$$[B_i^{(\beta)}] = \begin{bmatrix} \left(\frac{\partial N_i^{(\beta)}}{\partial x}\right) & 0 \\ 0 & \left(\frac{\partial N_i^{(\beta)}}{\partial y}\right) \\ \left(\frac{\partial N_i^{(\beta)}}{\partial y}\right) & \left(\frac{\partial N_i^{(\beta)}}{\partial x}\right) \end{bmatrix} \text{ with } i=1, 2 \tag{6}$$

The resulting stiffness matrix of the embedded discontinuous element can be written as

$$\begin{array}{c} \begin{array}{|c|} \hline 8 \\ \hline \end{array} \begin{array}{|c|} \hline 8 \\ \hline \end{array} \begin{array}{|c|} \hline 4 \\ \hline \end{array} \begin{array}{|c|} \hline 1 \\ \hline \end{array} \begin{array}{|c|} \hline 1 \\ \hline \end{array} \\ \begin{array}{|c|} \hline 4 \\ \hline \end{array} \end{array} \begin{array}{|c|} \hline K_{\alpha\alpha}^e = \\ \int_{\Omega} \mathbf{B}^{(\alpha)T} : \mathbf{L} : \mathbf{B}^{(\alpha)} d\Omega \\ \hline K_{\beta\alpha}^e = \\ \int_{\Omega} \mathbf{B}^{(\beta)T} : \mathbf{L} : \mathbf{B}^{(\alpha)} d\Omega \\ \hline \end{array} \begin{array}{|c|} \hline K_{\alpha\beta}^e = \\ \int_{\Omega} \mathbf{B}^{(\alpha)T} : \mathbf{L} : \mathbf{B}^{(\beta)} d\Omega \\ \hline K_{\beta\beta}^e = \\ \int_{\Omega} \mathbf{B}^{(\beta)T} : \mathbf{L} : \mathbf{B}^{(\beta)} d\Omega \\ + \int_{\Gamma_{db}} \mathbf{N}^{(\beta)T} : \eta : \mathbf{N}^{(\beta)} d\Gamma \\ \hline \end{array} \begin{array}{|c|} \hline \Delta \bar{\mathbf{u}} \\ \hline \Delta \bar{\mathbf{d}} \\ \hline \end{array} \begin{array}{|c|} \hline \Delta f_{\alpha} \\ \hline \Delta f_{\beta} \\ \hline \end{array} \tag{7}$$

2.3 Dual mapping integration

If there are discontinuous regions in a finite element, a normal 2×2 Gauss integration for a 4-node quadrilateral finite element can not be used to properly consider the embedded discontinuity. Therefore, integration of each element volume divided by the embedded discontinuous line is needed. This integration can be executed by means of dual mapping (Wan 1990). The dual mapping shown in Fig. 4 is a practical application of Gauss integration achieved by integration of a

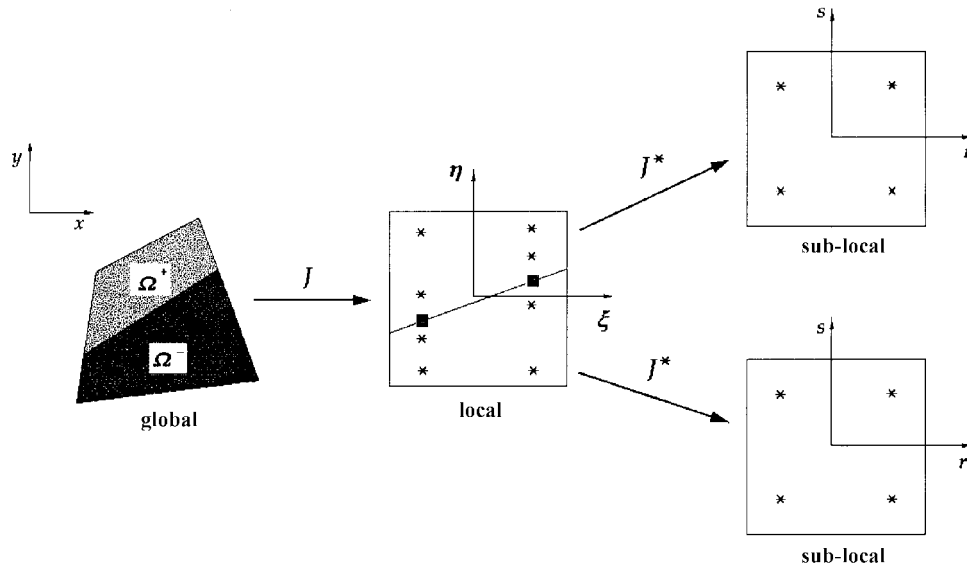


Fig. 4 Dual mapping technique

discontinuous quadrilateral element with 10 integration points. More specifically, integration of an element stiffness matrix of cracked element K_{ij}^e is carried out at each region using Eq. (8).

$$K_{ij}^e = \sum_{i=1} \sum_{j=1} K_{ij}^{e+}(r_i, s_j)(\det J_{ij})(\det J_{ij}^*)w_iw_j + \sum_{i=1} \sum_{j=1} K_{ij}^{e-}(r_i, s_j)(\det J_{ij})(\det J_{ij}^*)w_iw_j \quad (8)$$

where ξ_i and η_j are local coordinates, r_i and s_j are sub-local coordinates, J is Jacobian transformation from global coordinates to local coordinates, J^* is Jacobian transformation from local coordinates to sub-local coordinates, and w_i and w_j are weighting values.

2.4 Constitutive equation of discontinuous line

When maximum tensile stress reaches predefined tensile strength at an integration point in an element, a discontinuous line is embedded into the element in the direction normal to the maximum stress. For simplicity, nonlinear behavior in compression is ignored and elasticity is assumed. As constitutive equations for the discontinuous line having crack opening displacement ω and crack slip displacement δ at a center node in a discontinuous line, tension and shear softening curves, which can be obtained quantitatively from fracture experiments on concrete (Kitsutaka and Mihashi 1998), are introduced as shown in Fig. 5. In Fig. 5, the total areas under tension and shear softening curves $f(\omega)$ and $g(\delta)$ are fracture energies G_{fI} (mode I) and G_{fII} (mode II), respectively. In Fig. 5, f_t is tensile strength, τ_t is shear strength, ω_c is critical crack opening displacement of the softening curve, and δ_c is critical slip displacement of the softening curve. If tension and shear stresses exist simultaneously, the interaction between tension and shear stresses have to be considered in the softening effect. However the interaction is ignored in this paper for simplicity. Then, the constitutive tensor for the discontinuous line is expressed as Eq. (9). The terms η_{mn} and η_{tt} in Eq. (9) are defined in Eqs. (10a) and (10b), respectively.

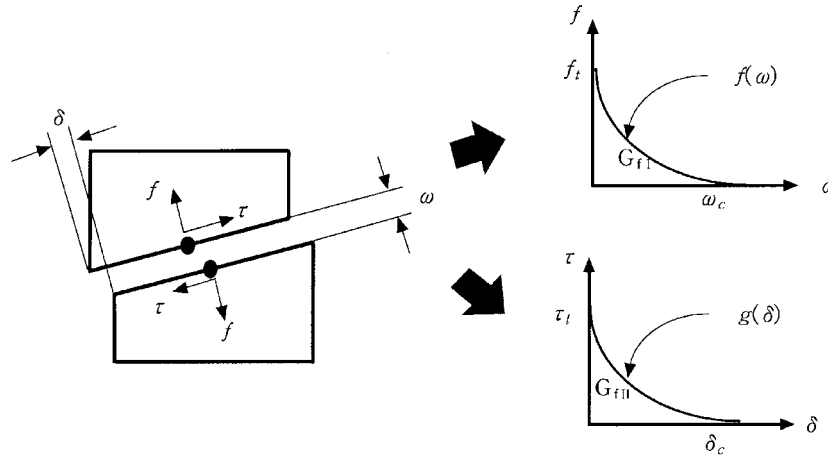


Fig. 5 Tension and shear softening curves of discontinuous line

$$\eta^e = \begin{bmatrix} \eta_{nn} & 0 \\ 0 & \eta_{tt} \end{bmatrix} \tag{9}$$

$$\eta_{nn} = \frac{\partial f(\omega)}{\partial \omega} \tag{10a}$$

$$\eta_{tt} = \frac{\partial g(\delta)}{\partial \delta} \tag{10b}$$

For the analysis, a nonlinear tension softening curve proposed by Hordijk based on fracture experiment of concrete (Kitsutaka and Mihashi 1998) is used. The equation is defined as

$$\frac{\sigma}{f_t} = \left\{ 1 + \left(C_1 \frac{\omega}{\omega_c} \right)^3 \right\} \exp\left(-C_2 \frac{\omega}{\omega_c} \right) - \frac{\omega}{\omega_c} (1 + C_1^3) \exp(-C_2) \tag{11}$$

where $C_1=3$ and $C_2=6.93$. Then, an idealized linear tension softening curve can be obtained simply by drawing a line tangential to the nonlinear tension softening curve, as shown in Fig. 6. Note that the slope of the linear softening model coincides with the initial slope of Hordijk’s nonlinear model. Then, η_{nn} and η_{tt} from Eq. (9) can be written for the analysis with the linear softening curves as Eqs. (12a) and (12b), respectively,

$$\eta_{nn} = -\frac{f_t}{\omega_{cL}} \tag{12a}$$

$$\eta_{tt} = -\frac{\tau_t}{\delta_{cL}} \tag{12b}$$

where f_t is tensile strength, ω_{cL} is critical crack opening displacement of the linear tension softening curve, τ_t is shear strength, and δ_{cL} is critical slip displacement of the linear shear softening curve.

2.5 Unloading path in softening curve

The major crack in concrete structure is assumed to be a crack that propagates more than other

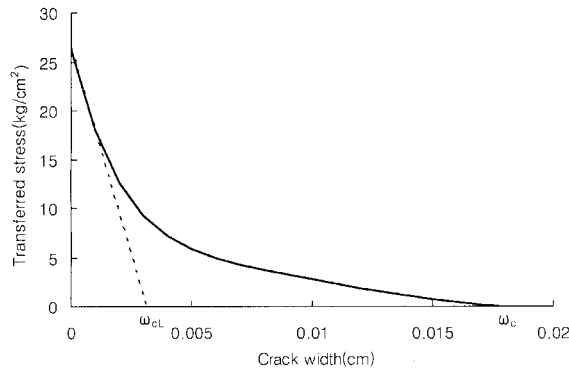


Fig. 6 Nonlinear and linear tension softening curves

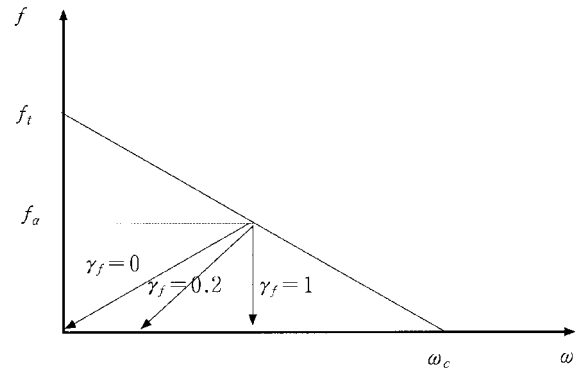


Fig. 7 Tension softening curve and unloading paths

distributed cracks. The major crack will therefore continue to grow and will ultimately cause the structure to fail. For concrete structure without a notch or a stress concentrator, initially distributed cracks tend to localize into the major crack simultaneous with closures of nearby distributed cracks. This localization can be simulated only when a proper localization algorithm is implemented in the analysis. A localization algorithm is implemented by using unloading path in the softening curve (Horii 1993). Various unloading paths can be considered in the softening curves (Reinhardt 1984). For example, possible three unloading paths in an idealized linear tension softening curve are shown in the Fig. 7 and can be written as

$$\omega = \left[\gamma_f + (1 - \gamma_f) \frac{\sigma}{f_\alpha} \right] \omega_\alpha \tag{13}$$

In Eq. (13), $\gamma_f=0$ defines the condition when the deformation is perfectly recovered as transfer stress normal to the crack surface reaches 0, and $\gamma_f=1$ defines the condition when the fracture deformation is unrecoverable, $\gamma_f=0.2$ represents partial recovery of the fracture deformation which is assumed in this study.

3. Applications and results

3.1 Double-notched tensile specimen

For the double-notched concrete specimen with given material properties shown in Fig. 8, fracture analysis is carried out to check mesh size objectivity of the embedded crack element. For simplicity, a linear tension-softening curve defined by the critical crack opening displacement ω_{cL} and the tensile strength f_t of concrete is used with the two different mesh configurations shown in Fig. 8. Fig. 9 shows that the load-displacement curves obtained from the failure analysis for two different mesh configurations are almost identical except for minor differences due to boundary constraints. If the boundary constraint effect is neglected, then global failure behaviors of the two mesh configurations become identical. It was further shown that numerical results obtained with the embedded crack approach were not sensitive to the mesh size and orientation (Wan 1990, Lofti and Shing 1995).

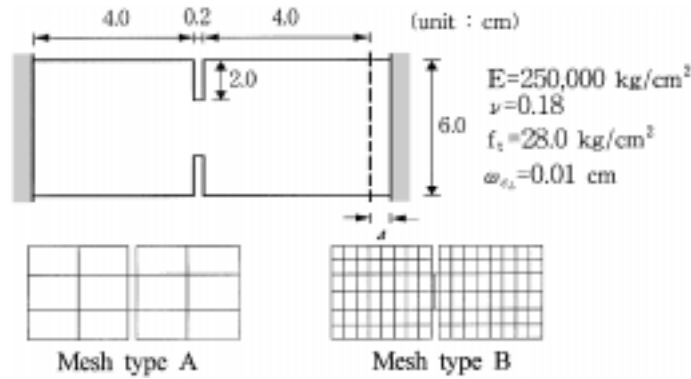


Fig. 8 Models for mesh size objectivity

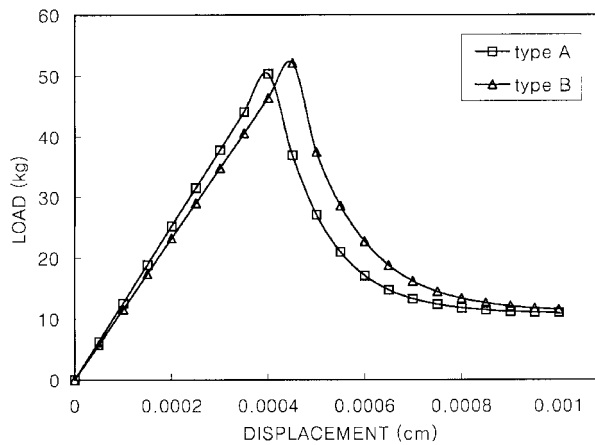


Fig. 9 Load-displacement responses

3.2 Beam specimen in tensile loading condition

A three point bending test specimen by Bazant and Gettu (1992) is used for a progressive fracture analysis of a concrete beam in tensile loading condition. The geometries and material properties of the single notched beam specimen are shown in Fig. 10. The finite element mesh refinement is shown in Fig. 11. For linear and nonlinear tension softening curves, $\omega_{cL}=0.01$ cm and $\omega_c=0.07$ cm are used in the analysis, respectively.

Fig. 12 compares the load versus vertical displacement at loading point between our analysis results, other fracture analysis result from Wu *et al.* (1998), and experimental data from Bazant and Gettu (1992). As shown in Fig. 12, the displacements corresponding to peak loads are very different between the analysis results and experimental result, although the peak loads from the three data are very close. These differences are due to the usage of given concrete elastic moduli and idealized boundary condition in the analyses which are different from those of the specimen in the experiment. It should be noted that large discrepancy in initial elastic stiffnesses of the load-displacement curves between the analytical results including the result by other analysis technique (Wu *et al.* 1998) and the experimental data has nothing to do with the failure analysis techniques

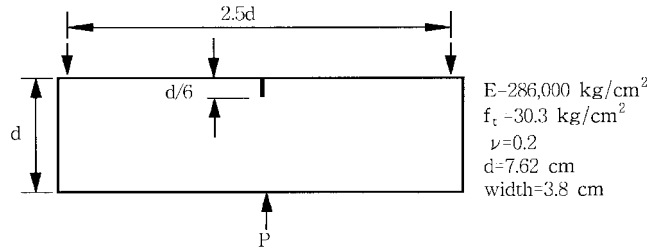


Fig. 10 Notched beam specimen under three point bending

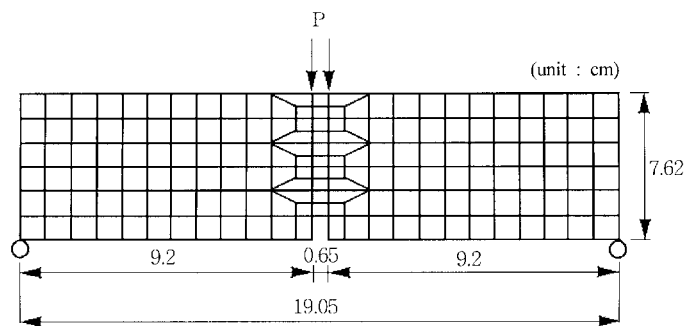


Fig. 11 Mesh refinement of notched beam specimen

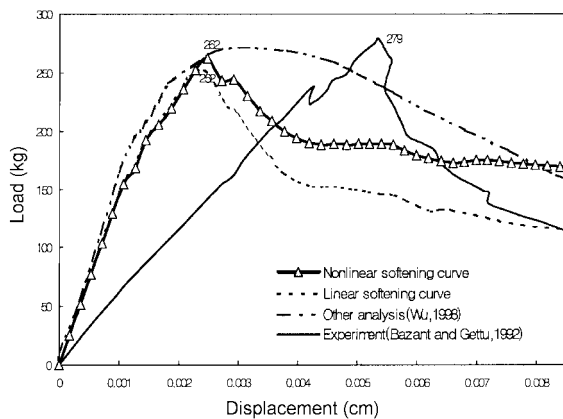


Fig. 12 Load-displacement responses

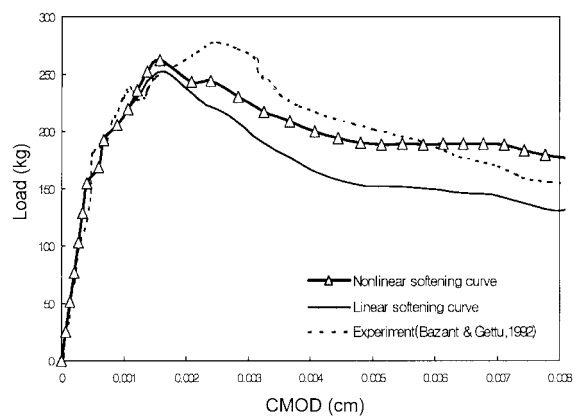


Fig. 13 Load-CMOD relationships

after cracking. The relationship between the load and CMOD (Crack Mouth Opening Displacement), which is a more reliable basis for the comparison, shows a good agreement with experimental results, as shown in Fig. 13. It can be seen that almost identical peak loads are obtained even when different softening curves are used. The post-peak result obtained with the nonlinear tension softening curve is slightly higher and closer to the experimental results than that obtained with the linear tension softening curve.

3.3 Beam specimen in mixed mode loading condition

In order to apply embedded crack elements to the fracture analysis of concrete under mixed mode loading, the concrete test specimen from Uchida *et al.* (1993) is selected for analysis (Fig. 14). The mesh refinement of mixed mode fracture specimen is shown in Fig. 15. For linear and nonlinear tension softening curves, $\omega_{c_l}=0.013$ cm and $\omega_c=0.09$ cm are used, respectively.

The experiment was executed in such a way that a localized failure in shear would be achieved by mixed mode loading (Uchida *et al.* 1993). From an experimental observation that the fracture energy of the mixed mode is slightly higher than that of mode I fracture, a linear shear softening curve for mode II producing the same amount of fracture energy as mode I is used in the analysis. A load-displacement response obtained from the analysis is compared with experimental results and shown in Fig. 16, while a comparison with other analysis result (Wu *et al.* 1998) is shown in Fig. 17. It can be seen that the analysis result on the load-displacement response including peak load shows good agreement with the experimental results and other analysis result, except for a slight discrepancy in initial elastic stiffnesses of the responses due to the aforementioned reasons. Both linear and nonlinear tension softening models give nearly identical results up to the peak load but a significant difference in the results occurs at post-peak stages, as shown in Fig. 17. As shown in Fig. 18, the direction of crack propagation changes according to the loading steps and heads toward the loading point coinciding with the direction observed from the experiment as described in step E in Fig. 18.

3.4 Pull out specimen

A pull out test specimen (Fig. 19) with lateral confinement from Ohlsson and Elfgren (1991) is selected to examine the performance of the localization algorithm with unloading path in softening curve. Finite element meshing is performed for only a half of the specimen utilizing the symmetry

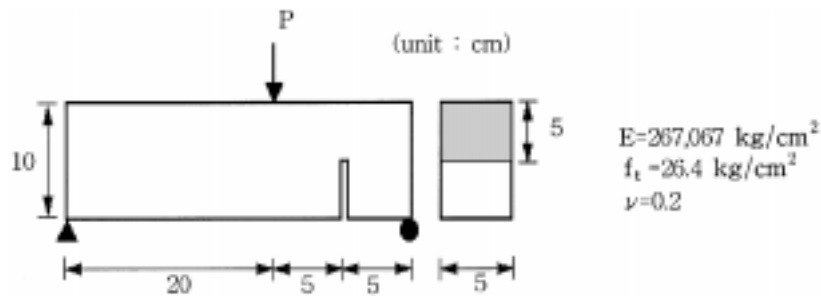


Fig. 14 Mixed mode fracture specimen

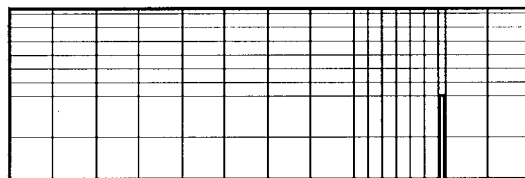


Fig. 15 Mesh refinement of specimen

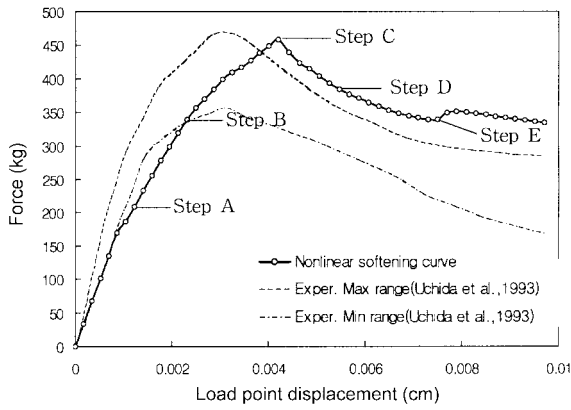


Fig. 16 Load-displacement responses

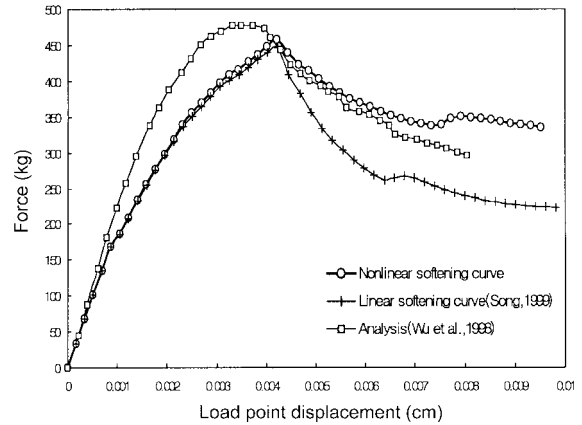


Fig. 17 Analytical load-displacement responses

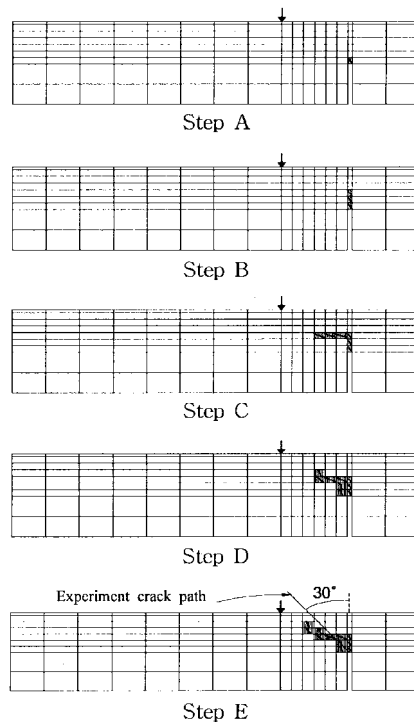


Fig. 18 Crack propagation under mixed mode loading

condition, as shown in Fig. 20. For linear and nonlinear tension softening curves, $\omega_{cL}=0.0041$ cm and $\omega_c=0.0285$ cm are used, respectively.

The load-displacement responses obtained from fracture analyses and experimental results are compared in Fig. 21. A comparison of the two analysis cases with and without the implementation of the unloading path is done. The analysis results indicate that the analysis effectively predicts global failure behavior of the concrete specimen observed in the experiment, but slightly underestimates peak load. It is also found that the aforementioned differences in deformations exist

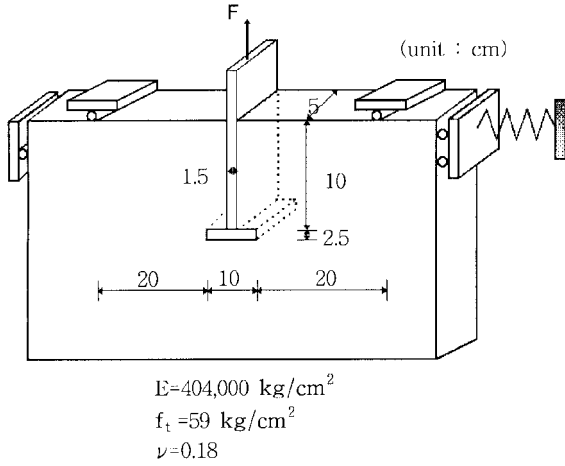


Fig. 19 Pull out test fracture specimen

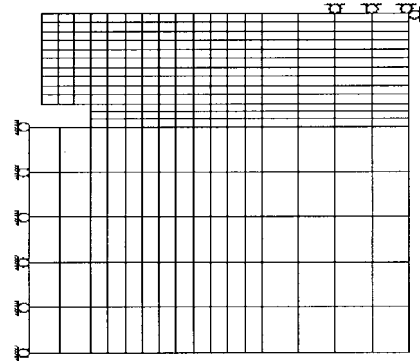


Fig. 20 Mesh refinement of pull out test specimen

for experimental and analytical results. Very close peak loads are obtained from the two analysis cases, although post-peak responses are very different. The sudden drop in the post-peak response predicted by the analysis with the nonlinear softening curve along with the unloading characteristics represents severe brittle failure due to the localization of cracks to a major crack simultaneous with closures of other cracks, which is shown in Fig 22. The simulation of the localized progressive failure obtained from the analysis, according to different loading steps as indicated in Fig. 21, is shown in Fig. 22. The first crack is formed in the element near the anchor, as shown at Step A in Fig. 22. The crack propagates progressively in a horizontal direction and the propagating direction of this major crack is changed toward the support at Step C. Vertical cracks on the anchor are also formed at Step B and propagate up to Step E, but they are closed as the major crack keeps propagating as shown at Step F. Eventually, failure occurs when the major crack reaches the support. In the steps F and G, the closing of vertical cracks on the anchor is clearly shown along with the progressively propagating fracture of the major crack in the horizontal direction.

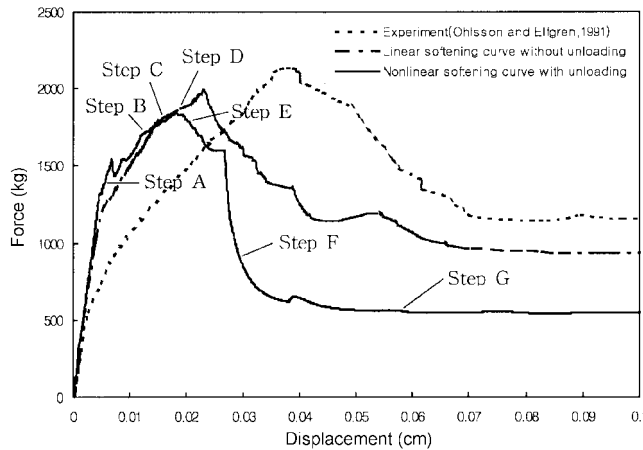


Fig. 21 Load-displacement responses

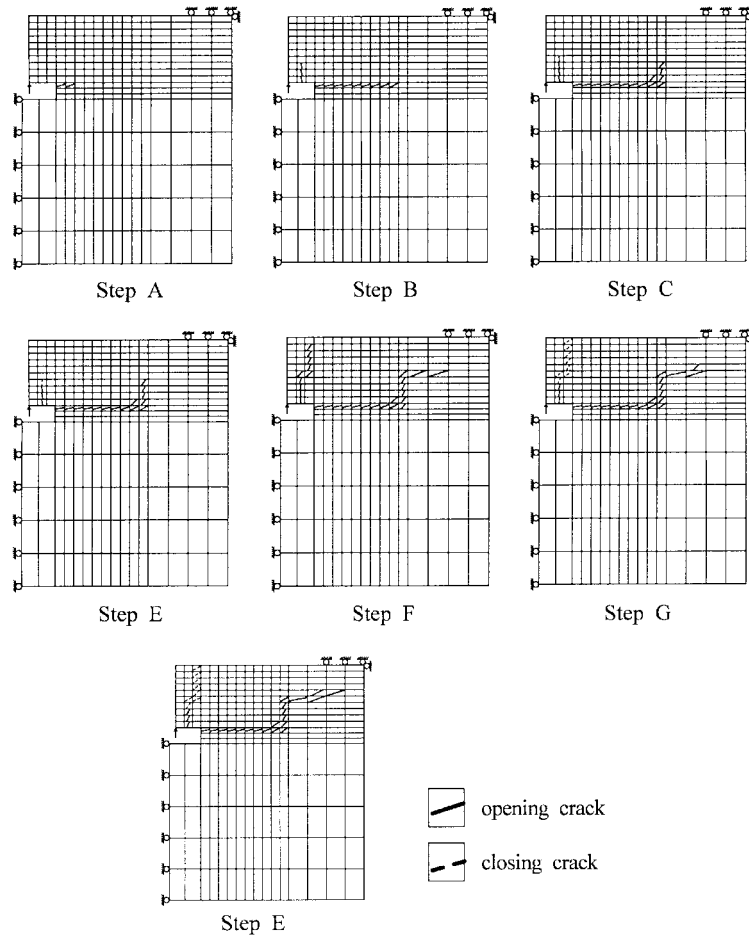


Fig. 22 Progressively propagating fracture

4. Conclusions

For the progressive fracture analysis of concrete, a finite element with embedded displacement discontinuity is utilized along with proper constitutive modeling of the fracture process zone in concrete. The performance of the so-called embedded crack approach for concrete fracture analysis is verified by several analytical examples on concrete specimens. It is shown that the embedded crack analysis retains mesh size objectivity and simulates localized failure without the major drawbacks of the discrete crack analysis. From the comparison of analytical results obtained with different softening curves, it has been shown that a simple idealized linear softening curve can be used to effectively predict the peak load of concrete structures. It has also been shown that the embedded crack approach is capable of predicting progressive fracture under mixed mode loading. By considering the unloading path in the softening curve as a localization algorithm, the localized progressive fracture is successfully simulated. It can be concluded that the embedded crack approach can be an effective alternative method to the smeared and discrete crack approaches.

References

- Ali, A. (1995), "FEM analysis of tensile fracture phenomena in concrete structures", *Fracture Mech. of Concrete Struct., Proc. FRAMCOS-2*, Wittmann, F. H., eds., Zurich, Switzerland, July, 1565-1574.
- Bazant, Z.P., and Gettu, R. (1992), "Rate effect and load relaxation in static fracture concrete", *ACI Mater. J.*, **89**(5), 456-468.
- Bocca, P., Carpinteri, A., and Valente, S. (1991), "Mixed mode fracture of concrete", *Int. J. Solids Struct.*, **27**, 1139-1153.
- Cervenka, V. (1970), "Inelastic finite element analysis of reinforced concrete panels", Ph.D. Dissertation, University of Boulder.
- Cope, R.J., Rao, P.V., Clark, L.A., and Norris, P. (1980), "Modelling of reinforced concrete behaviour for finite element analysis of bridge slabs", *Numerical Methods for Non-linear Problems*, Taylor et al., eds., Pineridge Press, Swansea, 457-470.
- de Borst, R., and Nauta, P. (1985), "Non-orthogonal cracks in a smeared finite element model", *Eng. Comput.*, **2**, 35-46.
- Dvorkin, E.N., and Assanelli, A.P. (1991), "2D finite elements with displacement interpolated embedded localization lines: the analysis of fracture in frictional materials", *Comput. Meth. in Appl. Mech. and Eng.*, **90**, 829-844.
- Horii, H. (1993), "Micromechanics and localization in concrete and rock", *Fracture and Damage of Concrete and Rock - FDCR-2*, Rosmanith, H. P., eds., E & FN Spon, 54-65.
- Kitsutaka, Y., and Mihashi, H. (1998), *Quantitative Evaluation Methods for Toughness and Softening Properties of Concrete, FRAMCOS-3 Pre-Conference Workshop*, Gifu, Japan, Oct. 11-12.
- Lofti, H.R., and Shing, P.B. (1995), "Embedded representation of fracture in concrete with mixed finite elements", *Int. J. Numer. Meth. Eng.*, **38**, 1307-1325.
- Malvern, L.E. (1969), *Introduction to the Mechanics of a Continuous Medium*, Prentice-Hall, New Jersey, 242-243.
- Matsuoka, S., Masuda, A., Takeda, Y., and Doi, S. (1999), "Analytical model for concrete structures influenced by crack initiation and propagation", *J. of Mater. Concrete Struct., Pavements, JSCE*, **620**, 1-13 (In Japanese).
- Ohlsson, U., and Elfgren, L. (1991), "Anchor bolts in concrete structures: Two-dimensional modeling", *Analysis of Concrete Structures by Fracture Mechanics, Proc. of the RILEM*, Elfgren, L., and Shah, S. P., eds., Chapman and Hall, London, 281-301.
- Okamura, H., and Maekawa, K. (1991), *Nonlinear Analysis and Constitutive Models of Reinforced Concrete*, Gihodo-Shuppan Co., Tokyo.
- Ngo, D., and Scordelis, A.C. (1967), "Finite element analysis of reinforced concrete beams", *J. American Concrete Inst.*, **64**(3), 152-163.
- Rashid, Y.R. (1968), "Analysis of prestressed concrete pressure vessels", *Nucl. Eng. Design*, **6**, 334-344.
- Reinhardt, H.W. (1984), "Fracture mechanics of an elastic softening material like concrete", *Heron, Delft*, **29**(2), 159-170.
- Uchida, Y., Rokuko, K., and Koyanagi, W. (1993), "Cracking behavior of concrete under mixed mode loading", *Proc. of 48th Annual Conference of JSCE*, **342**, 710-711 (In Japanese).
- Wan, R.G. (1990), "Finite element simulation of shear band development in geological media", Ph.D. Dissertation, University of Alberta, Canada.
- Wan, R.G., Chan, D.H., and Morgenstern, N.R. (1990), "A Finite element method for the analysis of shear bands in geomaterials", *Finite Elements in Analysis and Design*, Elsevier, **7**, 129-143.
- Wu, Z., Machida, A., and Gao, D. (1998), "Development of mixed finite element method for composite discontinuous analysis", *J. of Mater. Concrete Struct., Pavements, JSCE*, **598**, 149-159.